SCIENCE CHINA Materials

ARTICLES

mater.scichina.com link.springer.com

Published online 14 March 2017 | doi: 10.1007/s40843-017-9014-9
Sci China Mater 2017, 60(4): 285–294

Inorganic cesium lead halide $CsPbX_3$ nanowires for long-term stable solar cells

Jin-Feng Liao, Wen-Guang Li, Hua-Shang Rao, Bai-Xue Chen, Xu-Dong Wang, Hong-Yan Chen and Dai-Bin Kuang*

ABSTRACT **ABX_3-type organic-inorganic hybrid halide perovskite materials have been recognized as promising candidates for optoelectronic applications. However, poor stability of organic-inorganic hybrid perovskite hinders their forward long-term utilization and hence an effective strategy is needed to replace the organic part with an inorganic cation. Herein, all inorganic $CsPbI_3$ nanowires with a diameter of 50–100 nm are synthesized on fluorine-doped tin oxide glass via a simple solution-dipping process, which are further transformed into $CsPbBr_3$ nanowires through a solution-phase halide exchange method. A phase change from non-perovskite to perovskite structure is observed during the ion substitution process of I^- by Br^-, which is elaborated by X-ray diffraction, absorption and photoluminescence spectra. We for the first time apply the as-formed $CsPbI_3$ and $CsPbBr_3$ nanowires into perovskite solar cells, yielding power conversion efficiency of 0.11% and 1.21%, respectively. The inorganic $CsPbBr_3$ nanowire solar cell shows impressive stability which still remains 99% of the initial power conversion efficiency even after 5500 h aging.**

Keywords: inorganic perovskite, nanowires, ion exchange, solar cells, long-term stability

INTRODUCTION

The past seven years have witnessed the rapid development of perovskite solar cells (PSCs), with the power conversion efficiency (PCE) rocketing to 22.1% [1] from the initial 3.8% [2], which strongly demonstrates that organic-inorganic hybrid halide perovskite (hybrid perovskite) is a family of promising materials for optoelectronic applications. Hybrid perovskites have been confirmed to possess numerous highly-appreciated properties, such as prominent sunlight absorption [3], long electron/hole diffusion lengths [4,5], ease and low cost fabrication [6], etc., which render them an ideal candidate for various applications in light-emitting devices (LEDs) [7], semiconductor laser [8], and photodetectors [9].

However, hybrid perovskites are highly sensitive to moisture [10], ultraviolet (UV) light [11], and heat [12], which hinders their forward application [13,14]. Lead halides are the usual degradation product of the hybrid perovskites [10,15], deteriorating the performance of the solar cells, stemming from the wide bandgap and poor electrical conductivity [16,17]. Fortunately, inorganic perovskites, cesium lead halides ($CsPbX_3$, X=Cl, Br, I) exhibit excellent compositional stability under thermal stress [18], among which $CsPbBr_3$ possesses an impressive humidity stability [19], showing promise on addressing those issues. Actually, pioneer work has already evidenced that $CsPbX_3$ (X=Br, I) perovskites also exhibit significant photoelectric properties. Perovskite $CsPbBr_3$ is a direct bandgap semiconductor with a bandgap of 2.3 eV [20] and is reported to possess not only a long electron lifetime of 2.5 μs but also a high electron mobility up to ~1000 $cm^2 V^{-1} s^{-1}$ [21], which far outweighs that of single crystals of $MAPbI_3$ (24 $cm^2 V^{-1} s^{-1}$) [5]. Moreover, of particular note is that cesium halide perovskites greatly outperform hybrid perovskites in terms of stability. It has been demonstrated that PSCs based on $CsPbBr_3$ are more resistant to humidity and light illumination in comparison with $MAPbBr_3$ [19]. As for $CsPbI_3$, the undesirable yellow phase (non-perovskite structure) is formed under ambient temperature [22] which shows only 0.09% in PCE due to an unfavorable wide bandgap [23].

Morphology control has been investigated to have significant effects on the photophysical and photochemical properties and it is highly recommended as a starting point to enhance the performance of the materials for optoelec-

MOE Key Laboratory of Bioinorganic and Synthetic Chemistry, School of Chemistry, Sun Yat-sen University, Guangzhou 510275, China
* Corresponding author (email: kuangdb@mail.sysu.edu.cn)

tronic applications [24]. For instance, hybrid perovskites in the form of nanowires have been already synthesized and applied into PSCs [25], LEDs [26], laser [27] and photodetectors [28] etc., on account of the prominent properties of nanowires, such as fast electron transportation [29], direct charge transfer pathway [30] and low charge recombination [31]. However, limited attempts have been devoted to the controllable synthesis of all inorganic halide perovskites with well-defined nanostructure. Very recently, one dimensional $CsPbX_3$ (X=I, Br, Cl) nanowires [32] and quasi 2D nanoplates [33] were synthesized respectively by modifying the hot-injection technique reported by Protesescu *et al.* [34], where the as-formed $CsPbX_3$ nanowires reveal temperature-dependent photoluminescence (PL) and the nanoplates present high photoluminescent quantum yields (PLQYs) up to 90%, both of which are deemed as ideal candidates for optoelectronic devices. However, it is well known that hot-injection technique requires rigorous experimental condition (high temperature, inert atmosphere) and the organic surfactant (oleic acid, oleylamine) bound to the surface is adverse to the charge carrier transportation [35,36], which leads to a foregoing purification step to remove such ligands before film fabrication. Moreover, it is still challenging to employ colloidal solution with specific morphology to assemble film on conductive substrate as a result of dissolution [35] and aggregation [37]. For this reason, it is of great significance to *in situ* synthesize all inorganic $CsPbX_3$ nanowires on conductive substrate directly without the assistance of organic surfactant.

Herein, we report the synthesis of $CsPbI_3$ and $CsPbBr_3$ nanowires on fluorine-doped tin oxide (FTO) glasses by a simple solution-dipping process and solution-phase halide exchange method, respectively. Scanning electron microscopy (SEM), X-ray diffraction spectra (XRD), absorption spectra (UV-vis) and PL spectra were used to investigate the conversion process from $CsPbI_3$ to $CsPbBr_3$ nanowires. It is interesting to note such exchange by dipping the $CsPbI_3$ nanowires/FTO glass into the methanol solution of CsBr and annealing at 150°C can not only induce the exchange of I^- to Br^-, but also result in the structure transformation from nonperovskite structure $CsPbI_3$ to perovskite structure $CsPbBr_3$. After the complete anion exchange of I^- to Br^-, the photovoltaic performance of the planar PSCs based on $CsPbBr_3$ nanowires is 10 times higher than that of $CsPbI_3$ nanowires. Furthermore, the current inorganic $CsPbBr_3$ nanowire solar cell shows excellent stability which remains 99% of the initial PCE even after 5500 h aging time at room temperature.

EXPERIMENTAL SECTION

Materials

Lead iodide (PbI_2, ≥98%), lead bromide ($PbBr_2$, ≥98%), 2, 2′, 7, 7′-tetrakis-(*N*, *N*-di-*p*-methoxyphenylamine)-9, 9′-spirobifluorene (spiro-OMeTAD), bis(trifluoromethane) sulfonamide lithium salt (Li-TFSi), 4-*tert*-butylpyridine (*t*-BP), chlorobenzene and dimethylformamide (DMF, anhydrous, 99.8%) were purchased from Sigma-Aldrich. Cesium bromide (CsBr, >99.9%), cesium iodide (CsI, >99.9%) and hydroiodic acid (HI, 57% *w*/*w*) were purchased from Aladdin. Dried methanol and ethanol were purchased from Guangzhou Chemical Reagent factory.

Synthesis of $HPbI_3$

$HPbI_3$ powders were synthesized according to a previously reported method [38] by dissolving PbI_2 (9.26 g, 20 mmol) and 57% *w*/*w* hydroiodic acid (4 mL, 30 mmol) into 30 mL DMF with stirring at room temperature for 2 h. The solvent was removed by evaporating the resulting solution at 60°C, and the precipitate was washed with excess ethanol before dried under vacuum for 24 h.

Synthesis of $CsPbI_3$ nanowires and $CsPbBr_3$ nanowires

Forty microliter of $HPbI_3$ precursor solution (1 mol L^{-1} dissolved in DMF) was firstly deposited onto FTO substrate by spin-coating at 5000 rpm for 60 s. This substrate was then dipped into a solution of 10 mg mL^{-1} CsI in methanol to form yellow $CsPbI_3$ nanowires. Subsequently, the $CsPbI_3$ nanowires film grown on FTO glass was dipped into a methanol solution of 10 mg mL^{-1} CsBr for different periods and then annealed at 150°C for 10 min. Here, all the $CsPbX_3$ (X=Br, I) samples were annealed at 150°C for 10 min except special explanation.

Fabrication of perovskite solar cells

FTO glasses were pre-patterned with 3 mol L^{-1} HCl and zinc powder before cleaned with deionized water, alcohol, and acetone successively via ultrasonic process. A compact TiO_2 layer was deposited on the FTO glass by spin-coating a colloidal TiO_2 solution at 3000 rpm for 30 s and 5000 rpm for 60 s before annealed at 500°C for 1 h. The TiO_2 colloid solution was prepared following our previous report [39]. After cooling down to room temperature, the compact TiO_2 film was immersed into 0.04 mol L^{-1} $TiCl_4$ aqueous solution for 30 min at 70°C and then heated to 500°C for 30 min. And then an $HPbI_3$ layer was prepared on the TiO_2 coated FTO by spin-coating. $CsPbI_3$ nanowires were obtained by

immersing the as-prepared $HPbI_3$ film into 10 mg mL^{-1} CsI methanol solution for 1 min and then annealed at 150°C for 10 min. As for $CsPbBr_3$ nanowire, the halide exchange was performed by dipping the $CsPbI_3$ nanowires film into 10 mg mL^{-1} CsBr solution in methanol for 5 min and then annealed at 150°C for 10 min. Then a hole-transport material solution consisting of spiro-OMeTAD (73.2 mg), Li-TFSi (9.1 mg) and *t*-BP (28.8 μL) and chlorobenzene (1 mL) was spin-coated onto the perovskite nanowires at 5000 rpm for 60 s. An Au layer with a thickness of 100 nm was deposited by magnetron sputtering.

Characterizations

The XRD patterns were recorded on RigakuCo. X-ray powder diffractometer (Cu Kα radiation, λ=1.5418 Å). A UV-vis-NIR spectrophotometer (Shimadzu UV-3600) was employed to measure the UV-vis absorption spectra. The morphology and composition of the samples were measured using a scanning electron microscope (SU8010) and an energy dispersive X-ray detector (IXRF), respectively. PL (excitation at 325 nm) was measured with Edinburgh Instruments LTD (FLSP980). The photovoltaic performance of PSCs was recorded using Keithley 2400 source meter with a scan rate of 0.15 V s^{-1} under one sun AM 1.5G (100 mW cm^{-2}) illumination with a solar light simulator (Oriel, Model:91192) which was calibrated with an NREL standard Si solar cell. And the active area of the cell was defined as 0.16 cm^2.

RESULTS AND DISSCUSSIONS

Synthesis of $CsPbI_3$ nanowires

A simple and facile solution-dipping method was developed to synthesize the $CsPbI_3$ nanowires on FTO glass substrate. As schemed in Fig. 1a, the $HPbI_3$ solution was spin-coated onto the FTO substrate first, followed by dipping into CsI methanol solution to assemble $CsPbI_3$ nanowires film. The $HPbI_3$ precursor was synthesized via the reaction of PbI_2 and HI according to the previous report [38]. The XRD pattern (Fig. S1) shows that the peak of PbI_2 at 12.7° shifts to 11.5° after reaction with HI as a result of an increased interlayer distance [38], and the atomic ratio of I to Pb is about 3:1 determined by energy dispersive X-ray spectra (EDX, Table S1), further indicating the successful synthesis of $HPbI_3$. Fig. 1b shows the morphology of the $HPbI_3$ film, which is constituted by discontinuous, large sized grains and this phenomenon was also found in a recent report [40]. After reaction with CsI, the parent $HPbI_3$ film turned yellow, and surprisingly, nanowires with diameters of 50–100 nm and lengths up to several micrometers tightly covered on the FTO glass could be observed (Fig. 1c and Fig. S2a). The XRD patterns of the products can be assigned to orthogonal phase $CsPbI_3$ (Fig. 2), with a non-perovskite structure (JCPDS Card No. 74-1970) [32].

Importance of $HPbI_3$ precursor in synthesis of $CsPbI_3$ nanowires

It should be noted that the $HPbI_3$ precursor played a vital

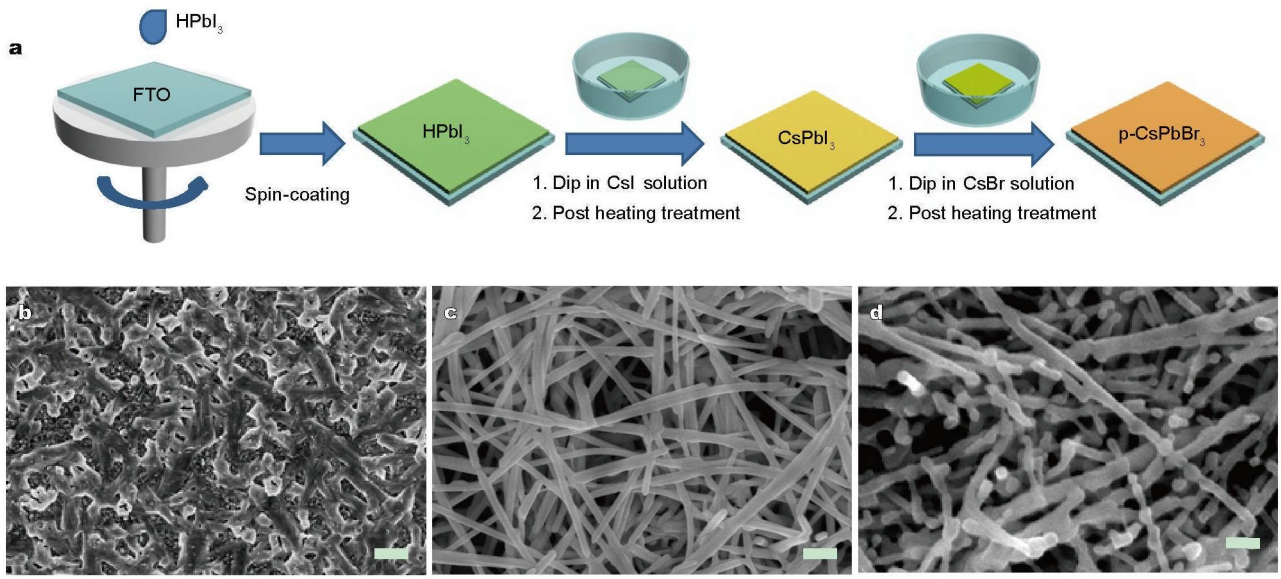

Figure 1 (a) Schematic illustration of the synthesis of $CsPbX_3$ nanowires, and SEM images of (b) $HPbI_3$ films, (c) $CsPbI_3$ nanowires film, and (d) $CsPbBr_3$ nanowires film. Scale bars are 200 nm. The prefix p represents a perovskite structure.

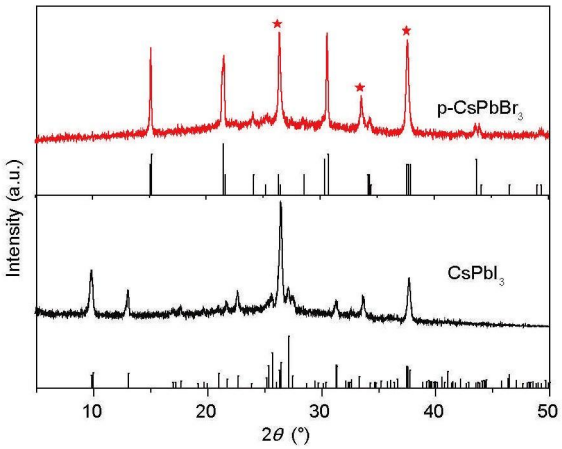

Figure 2 XRD patterns of the as-formed $CsPbI_3$ nanowires by solution-dipping method and $CsPbBr_3$ obtained by halide exchange in comparison with standard XRD pattern. Peaks marked with an asterisk are XRD signals assigned to the FTO substrate.

role in the synthesis of $CsPbI_3$ nanowires. Attempt using the typical PbI_2 precursor film was conducted by dipping into CsI methanol solution. However, the XRD patterns (Fig. S3a) show that the peak of PbI_2 at 12.7° is still clearly observed after a long dipping time even though morphology of the obtained nanowires (Fig. S3b) indicates the incomplete conversion. In contrast, the reaction of $HPbI_3$ with CsI was astonishingly fast. $CsPbI_3$ was formed within 5 s and the XRD peak of $HPbI_3$ disappeared (Fig. S3c). Here, $HPbI_3$ having a faster complete reaction with CsI could be attributed to an increased layer lattice, which facilitated the reaction with CsI to form $CsPbI_3$ [38,40].

Synthesis of $CsPbBr_3$ nanowires via halide exchange

As mentioned above, nonperovskite $CsPbI_3$ is not beneficial for fabricating PSCs and it requires a high temperature (335°C) to convert to the black phase, which will revert to yellow phase after cooling down at ambient temperature [22]. Concerning that perovskite $CsPbBr_3$ possesses a superior stability than $CsPbI_3$ in ambient atmosphere, thus we look forward to converting the $CsPbI_3$ to $CsPbBr_3$ with the nanowires morphology maintained. The halide exchange process was performed by exposing the as-formed $CsPbI_3$ nanowires film into CsBr methanol solution and then annealed at 150°C for 10 min (Fig. 1a).

The accomplishment of the anion substitution of I^- by Br^- was accompanied by the color of the film turning to orange ($CsPbBr_3$) from the inchoative pale yellow of $CsPbI_3$. The XRD patterns in Fig. 2 confirm the formation of orthogonal phase $CsPbBr_3$, with a perovskite structure (JCPDS Card No. 72-7929) [19,32]. Highlighted in Fig. 1d and Fig. S2b, the $CsPbBr_3$ nanowires were successfully synthesized by anion exchange, with diameters merely changed to 50–200 nm. Compared with the $CsPbI_3$, the $CsPbBr_3$ nanowires showed an uneven diameter and a rougher surface. The slight morphology variation is probably attributed to the crystal structural change from nonperovskite to perovskite structure during the halide exchange of I^- by Br^-. The PbI_6 octahedra are isolated in the nonperovskite $CsPbI_3$, while $PbBr_6$ octahedra are connected in the perovskite $CsPbBr_3$ structure, which will be further discussed below. Cross-sectional SEM images (Fig. S4) illustrate the thickness variation between the as-prepared materials. The thickness of $HPbI_3$ film on FTO glass is ca. 300 nm (Fig. S4a), while after reaction with CsI, the thickness was almost doubled (Fig. S4b). Nevertheless, the thickness no longer changes during the Br substitution process (Fig. S4c).

The advent of ion substitution was proposed to figure out the difficulties in direct synthesis of materials with a specific morphology [41]. Here, an expectation of direct synthesis of $CsPbBr_3$ nanowires on FTO glass substrate was terminated by the trial of dipping the $HPbI_3$ film/FTO into a CsBr methanol solution straightly. XRD patterns (Fig. S5a) evidence the formation of perovskite structure $CsPbBr_3$ after dipping for 5 min, while the SEM image, presented in Fig. S5b indicates the morphology of cubes with a diameter of hundreds of nanometer was acquired instead of nanowires, which underlines the necessity of sacrificing the $CsPbI_3$ nanowires as templates for the sake of $CsPbBr_3$ nanowires.

Studies of anion exchange via XRD, UV-vis and PL

Anion exchange in cesium lead halide perovskite nanocrystals [42,43] has been demonstrated, while it has been rarely studied in bulk films [37]. To further gain insight into the ion exchange dynamics of the conversion reaction from $CsPbI_3$ to $CsPbBr_3$, XRD patterns of the $CsPbI_3$ nanowires film as a function of dipping time into CsBr solution were measured. Fig. 3a indicates that, at the initial 20 s, no emerging XRD signals was detected, implying a similar crystallographic structure of nonperovskite $CsPbI_3$ was maintained but a magnification of XRD patterns (Fig. S6) showed that the XRD peaks of $CsPbI_3$ located at 9.9° and 13.1° were gradually shifted to higher angles at 10.1° and 13.3° with increasing dipping time respectively, indicating that I substituted by smaller atom Br and nonperovskite $CsPbI_{3-x}Br_x$ was formed within such a short dipping time.

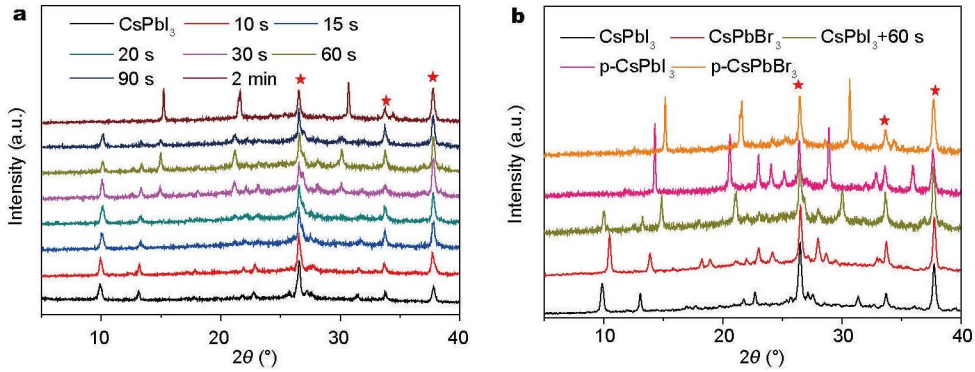

Figure 3 (a) XRD pattern of $CsPbI_3$ nanowires film dipped in CsBr solution for varying time. (b) XRD pattern of the sample with dipping time of 60 s was compared with that of nonperovskite and perovskite $CsPI_3$ and $CsPbBr_3$. Peak marked with an asterisk are XRD signals assigned to FTO substrate.

Extending the dipping time to 30 s till 90 s, several distinct emerging peaks at 14.9°, 21.1° and 30.1° could be easily observed. A further analysis by comparing CsBr solution for 60 s with that of both perovskite structure $CsPbX_3$ (X=I, Br) and nonperovskite structure $CsPbX_3$ (X=I, Br; Fig. 3b) suggested both two phases of $CsPbI_{3-x}Br_x$ (perovskite structure and nonperovskite structure) coexisted since the XRD peaks of intermediate product stood at the middle of the corresponding peaks of $CsPbI_3$ and $CsPbBr_3$. Whereafter, with dipping time increased to 2 min, a pure orthorhombic perovskite $CsPbBr_3$ was obtained, characterized with XRD patterns (Fig. 2) [19, 35]. Further prolonging the dipping time (e.g., >2 min) did not show any difference in XRD patterns (Fig. S7a), indicating the complete conversion of I^- to Br^-.

In order to explore the exact role of the post heat treatment in the aforementioned halide exchange process, we also measured XRD patterns of $CsPbI_3$ dipped in CsBr solution for varying time but without a post thermal treatment (Fig. S8a). The magnified of XRD patterns (Fig. S8b), reveal that the XRD signals of $CsPbI_3$ at 9.9° and 13.1° shifted to higher angles of 10.4° and 13.8° respectively after exposed to CsBr solution for 2 min, and no variations appeared to the XRD patterns as dipping process continued (Fig. S8c). Whereas, after the complete conversion, the color of the $CsPbI_3$ film turned from the initial yellow to white and the XRD patterns of the final white product can be assigned as orthorhombic $CsPbBr_3$ with a nonperovskite structure (Fig. S8d, JCPDS Card No. 74-2251), which is different from the results obtained by the halide process including a post heat treatment schemed in Fig. 1a. In addition, no XRD peaks of perovskite structure $CsPbX_3$ could be found during the ion substitution without a post heat treatment process (Fig. S8a), suggesting that the post heat treatment was necessary to form the perovskite structure $CsPbX_3$. In other words, the nonperovskite $CsPbI_3$ was transferred into the nonperovskite $CsPbBr_3$ after dipped into CsBr solution for 2 min, and a following post heat treatment (annealing at 150°C for 10 min) enabled the phase change from nonperovskite $CsPbBr_3$ to perovskite structure $CsPbBr_3$, which was further proved by the temperature dependence XRD patterns of the as-formed nonperovskite structure $CsPbBr_3$ (Fig. S9). There is no variation in the XRD patterns until the temperature was raised to 150°C, and then the XRD peaks of perovskite $CsPbBr_3$ appeared while that of nonperovskite $CsPbBr_3$ disappeared.

As schemed in Fig. 4, we can make a conclusion for the halide exchange process including a post heat treatment, that nonperovskite $CsPbI_{3-x}Br_x$ was formed within 30 s; both two phases of $CsPbI_{3-x}Br_x$ (nonperovskite structure and perovskite structure) coexisted during 30–90 s; after 2 min the full conversion from $CsPbI_3$ to $CsPbBr_3$ was achieved with a phase change from initial nonperovskite to perovskite structure.

Transformation in crystal structure is always accompanied with photophysical properties variation [44]. In this regard, the absorption spectra of the $CsPbI_3$ nanowires films as a function of dipping time into CsBr methanol solution were characterized (Fig. 5a). The absorption onset of solution-phase synthesized $CsPbI_3$ nanowires locates at 449 nm with a bandgap of 2.78 eV from Tauc plot (Fig. S10), which matches well with the previous report [19]. After ion substitution completed, the as-formed $CsPbBr_3$ perovskite exhibited an absorption onset at 540 nm with a band gap of 2.30 eV. The rightmost blue solid line in Fig. 5a represents the absorption spectra of perovskite structure $CsPbI_3$ (obtained by heating the as-formed $CsPbI_3$ nano-

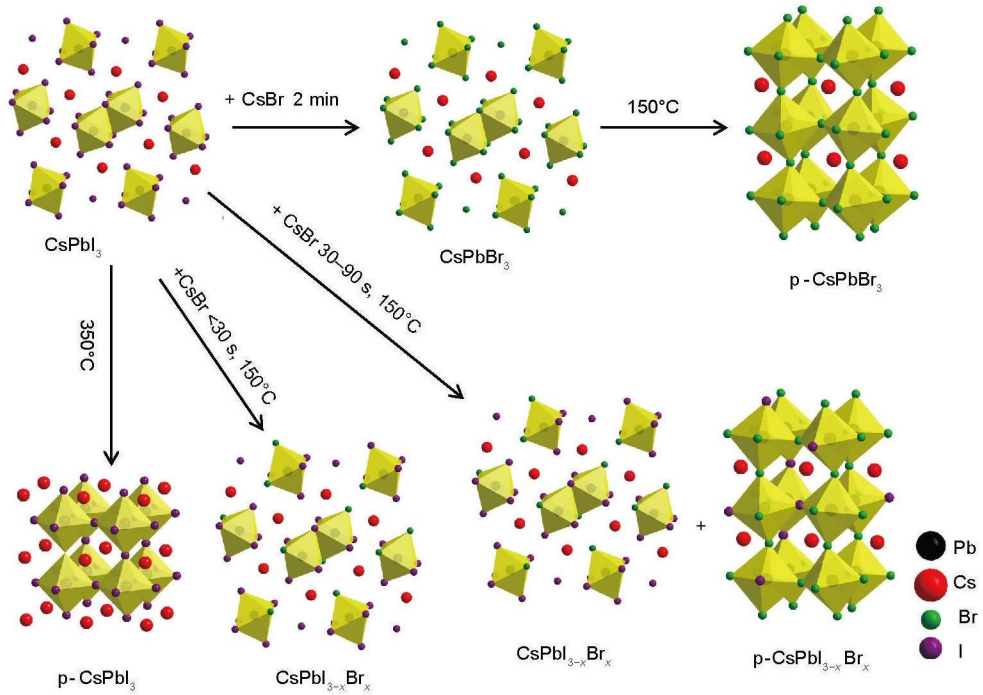

Figure 4 The schematic diagram of structure conversion from nonperovskite $CsPbI_3$ to perovskite $CsPbBr_3$.

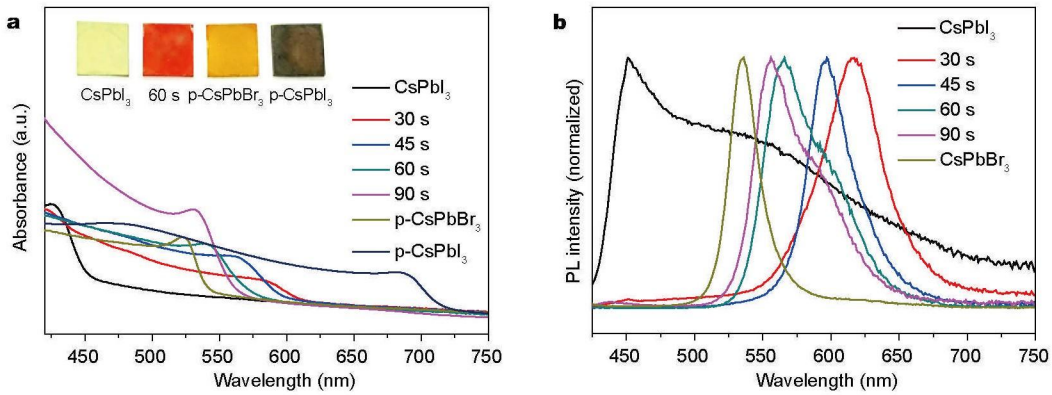

Figure 5 (a) Absorption spectra and (b) normalized PL spectra of $CsPbI_3$ nanowires films dipped in CsBr solution for varying time. The inset photographs are $CsPbI_3$, $CsPbI_3$ film with dipping time of 60 s, p-$CsPbBr_3$ and p-$CsPbI_3$ films from left to right, respectively.

wires film at 350°C) with an absorption onset at 700 nm and a bandgap of 1.7 eV (Fig. S10). It is interesting to note that the halide-exchange intermediate products (dipping time from 30 to 90 s) possess a wider absorption range than the initial material $CsPbI_3$ and the final product $CsPbBr_3$. More specifically, after dipped in CsBr solution for 30 s, the absorption onset of the $CsPbI_3$ film shifts to around 615 nm, and towards to 600 nm (for 45 s), 581 nm (for 60 s) and 570 nm (for 90 s) gradually as I^- substitution continued, and finally towards the onset of $CsPbBr_3$ 540 nm with the shift ceased as dipping time advances (Fig. S7b). Studies about $CsPbX_3$ nanocrystals halide exchange have illustrated that the absorption onset of the perovskite structure $CsPbI_{3-x}Br_x$ can be varied from 520–700 nm by adjusting the atom ratio of Br to I [42,43], and therefore it can be concluded that the perovskite structure $CsPbI_{3-x}Br_x$ intermediate was formed, which is consistent with the aforementioned XRD analysis in Fig. 3b. The inset photographs in Fig. 5a display the color variation of the as-prepared $CsPbI_3$ nanowires film after dipping into CsBr solution or heat treatment. The pale yellow film was the as-prepared $CsPbI_3$ nanowires, and after dipped into CsBr solution for 60 s, the film was red as a result of the formation of perovskite $CsPbI_{3-x}Br_x$ but the final product perovskite $CsPbBr_3$ nanowires was or-

ange and the black film was the perovskite $CsPbI_3$ film. The above analysis demonstrated that perovskite structure $CsPbI_{3-x}Br_x$ with a tunable bandgap can be formed via a careful control of the dipping time.

Corresponding to UV-vis, PL spectra also witnessed such interesting phenomenon in optical spectrum, as shown in Fig. 5b. The PL spectrum of the as-prepared $CsPbI_3$ nanowires consists of two peaks centered at 450 and 540 nm. The narrow peak is assigned as the band edge emission while the broad peak has been previously attributed to the formation of self-trapped excitons [32]. The temperature-dependent PL spectra of $CsPbI_3$ NWs in Fig. S11 reveal that the exciton emission peak of $CsPbI_3$ red-shifts with increasing temperature from 100 to 298 K, which is consistent with the formation of self-trapped exciton which can produce strong electron-phonon coupling contribution to dictate band gap behavior [32]. Similar to the UV-vis spectra, as dipping time extending from 30 to 90 s, the PL peaks shift from 620 to 560 nm. The PL emission peak of the final product is located at 538 nm indicating the as-formed $CsPbBr_3$ nanowires are PL active, with a narrow full-width of half maximum (FWHM) about 40 nm. Further prolonging the dipping time to more than 2 min, no differences between the PL peaks position are observed, indicating full halide exchange from $CsPbI_3$ to $CsPbBr_3$ (Fig. S7c).

Photovoltaic performance of PSCs based on $CsPbX_3$ nanowires

The optoelectronic application of perovskite material is becoming a recent research hotspot. In this regard, the current *in-situ* growth of $CsPbI_3$ and $CsPbBr_3$ nanowires are further applied to the PSCs. To elucidate that such method has a favorable reproducibility, ten independent devices based on $CsPbI_3$ and $CsPbBr_3$ nanowires were measured, respectively (as shown in Fig. S12). Fig. 6a shows the current density-voltage curves of both solar cells based on $CsPbI_3$ and $CsPbBr_3$ nanowires. As listed in Table 1, the performance of device based on $CsPbI_3$ yields a short circuit current density (J_{SC}) of 0.415 mA cm^{-2}, an open circuit voltage (V_{OC}) of 643 mV, a fill factor (FF) of 0.429, and a PCE of 0.11%. By contrast, the device based on $CsPbBr_3$ nanowires formed by anion exchange achieves a J_{SC} of 2.96 mA cm^{-2}, a V_{OC} of 851 mV, an FF of 0.445 and a PCE of 1.21%. It is very interesting to note that more than tenfold enhancement in the PCE is achieved by the substitution of I^- by Br^-. The PCE of the devices based on $CsPbI_{3-x}Br_x$ intermediate formed in the conversion process was measured with an inferior performance compared with pure $CsPbBr_3$, properly owning to the existence of nonperovskite counterpart serving as traps limiting the photovoltaic properties. Fig. 6b presents the cross-sectional SEM image of the device based on $CsPbBr_3$ nano-

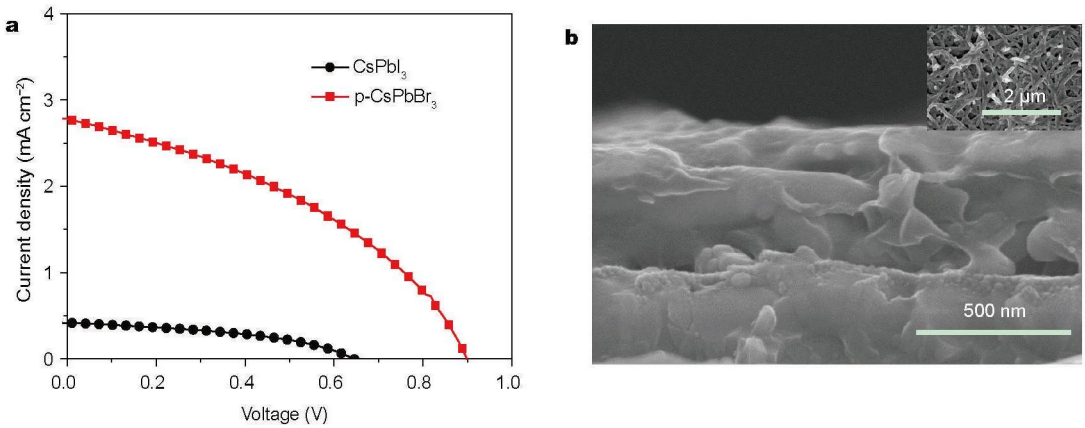

Figure 6 (a) *J-V* characteristics of the PSC devices and (b) cross-sectional and plane-view (inset image) SEM images of a full cell based on $CsPbBr_3$ nanowires.

Table 1 Device parameters of PSCs

	J_{SC} (mA cm^{-2})	V_{OC} (mV)	PCE (%)	FF
$CsPbI_3$ nanowires	0.415	643	0.11	0.429
p-$CsPbBr_3$ nanowires	2.96	851	1.21	0.445

wires (FTO glass/TiO_2 compact layer/$CsPbBr_3$ nanowires/spiro-OMeTAD/Au) while the inset SEM image

in Fig. 6b is the plane-view image of the device based on $CsPbBr_3$, where nanowires can be easily seen revealing that spiro-OMeTAD does not form a top layer upon the nanowires film but fills the empty space among nanowires, as does Au electrode. Moreover, there is no distinct layer boundary between the $CsPbBr_3$ nanowires with spiro-OMeTAD and Au electrode from the cross-sectional SEM image. Therefore, these inferior performances are mainly attributed to the insufficient coverage of the random $CsPbX_3$ nanowires on the substrate, which causes a direct contact between c-TiO_2 with spiro-OMeTAD or Au electrode resulting in the electron-hole recombination [45]. On the other hand, nanowires with an incomplete coverage on substrate will lead to a great loss in light harvesting, thus a decrease in J_{SC} [46]. For comparison, solar cells based on cube-based $CsPbBr_3$ films were fabricated with the same configuration. Table S2 summarized the photovoltaic metrics of 8 devices based on cubed-based $CsPbBr_3$ film with an average PCE of 0.14%, which is lower than that of $CsPbBr_3$ nanowires. By contrast, the better performance can be attributed to prominent properties of nanowires, such as fast electron transportation and direct charge transfer pathway.

Long-term stability of PSCs based on $CsPbX_3$ nanowires

The stability of solar cell is a crucial issue for the commercial application. Till today, the long-time stability of organic-inorganic PSC is still unsatisfactory and required to be resolved urgently. Herein, the stability study of the inorganic $CsPbI_3$ and $CsPbBr_3$ nanowire planar perovskite solar cell is further performed. Fig. 7 presents the normalized stability curves of both $CsPbI_3$ and $CsPbBr_3$ nanowire solar cells, which highlight that the current inorganic perovskite solar cells are highly stable even after around 5500 h aging at ambient condition in dark. Such impressive stability of inorganic perovskite nanowire solar cells will potentially stimulate the wide applications.

CONCLUSIONS

In summary, we reported a simple solution-dipping method and halide exchange technique to synthesize the $CsPbI_3$ and $CsPbBr_3$ nanowires grown on FTO glass, respectively. Herein, SEM, XRD patterns, UV-vis spectra and PL spectra studies reveal that the nonperovskite structure $CsPbI_3$ is transferred into nonperovskite structure $CsPbI_{3-x}Br_x$ as the first step of the halide conversion, and then perovskite structure $CsPbI_{3-x}Br_x$ appears together before the complete conversion to perovskite structural $CsPbBr_3$. PSC devices based on $CsPbI_3$ and $CsPbBr_3$ nanowires reached a PCE of 0.11% and 1.21%, respectively, and both exhibited impressive stability over 5500 h. Further studies on the thickness optimization of the $CsPbX_3$ nanowires and inorganic-organic hybrid $MAPbX_3$ nanowires are expected to obtain both high efficiency and good stability PSCs. Additionally, this work provides a simple solution-phase synthesis method to the *in situ* synthesis of the inorganic perovskite nanowires, which will stimulate the great potentials in semi-transparent perovskite solar cells, photodetectors and other optoelectronics.

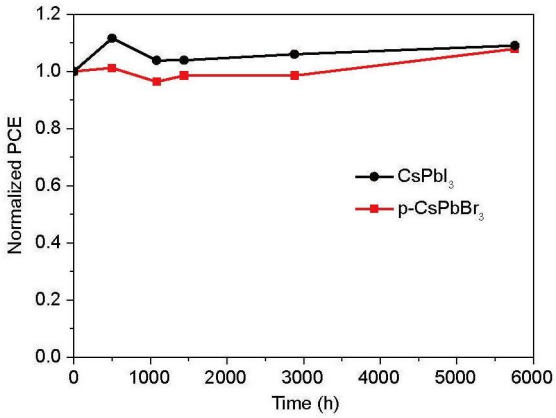

Figure 7 Normalized PCE for devices based on $CsPbI_3$ and p-$CsPbBr_3$ nanowires as a function of aging time.

Received 20 January 2017; accepted 24 February 2017; published online 14 March 2017

1 http://www.nrel.gov/ncpv/images/efficiency_chart.png
2 Kojima A, Teshima K, Shirai Y, *et al.* Organometal halide perovskites as visible-light sensitizers for photovoltaic cells. J Am Chem Soc, 2009, 131: 6050–6051
3 Im JH, Lee CR, Lee JW, *et al.* 6.5% efficient perovskite quantum-dot-sensitized solar cell. Nanoscale, 2011, 3: 4088–4093
4 Stranks SD, Eperon GE, Grancini G, *et al.* Electron-hole diffusion lengths exceeding 1 micrometer in an organometal trihalide perovskite absorber. Science, 2013, 342: 341–344
5 Dong Q, Fang Y, Shao Y, *et al.* Electron-hole diffusion lengths > 175 m in solution-grown $CH_3NH_3PbI_3$ single crystals. Science, 2015, 347: 967–970
6 Chen BX, Rao HS, Li WG, *et al.* Achieving high-performance planar perovskite solar cell with Nb-doped TiO_2 compact layer by enhanced electron injection and efficient charge extraction. J Mater Chem A, 2016, 4: 5647–5653
7 Tan ZK, Moghaddam RS, Lai ML, *et al.* Bright light-emitting diodes based on organometal halide perovskite. Nat Nanotech, 2014, 9: 687–692

8 Xing G, Mathews N, Lim SS, *et al.* Low-temperature solution-processed wavelength-tunable perovskites for lasing. Nat Mater, 2014, 13: 476–480
9 Dou L, Yang YM, You J, *et al.* Solution-processed hybrid perovskite photodetectors with high detectivity. Nat Commun, 2014, 5: 5404
10 Li B, Fei C, Zheng K, *et al.* Constructing water-resistant $CH_3NH_3PbI_3$ perovskite films via coordination interaction. J Mater Chem A, 2016, 4: 17018–17024
11 Leijtens T, Eperon GE, Pathak S, *et al.* Overcoming ultraviolet light instability of sensitized TiO_2 with meso-superstructured organometal tri-halide perovskite solar cells. Nat Commun, 2013, 4: 2885
12 Conings B, Drijkoningen J, Gauquelin N, *et al.* Intrinsic thermal instability of methylammonium lead trihalide perovskite. Adv Energ Mater, 2015, 5: 1500477
13 Chen J, Liu D, Al-Marri MJ, *et al.* Photo-stability of $CsPbBr_3$ perovskite quantum dots for optoelectronic application. Sci China Mater, 2016, 59: 719–727
14 Wei J, Shi C, Zhao Y, *et al.* Potentials and challenges towards application of perovskite solar cells. Sci China Mater, 2016, 59: 769–778
15 Niu G, Li W, Meng F, *et al.* Study on the stability of $CH_3NH_3PbI_3$ films and the effect of post-modification by aluminum oxide in all-solid-state hybrid solar cells. J Mater Chem A, 2014, 2: 705–710
16 Berhe TA, Su WN, Chen CH, *et al.* Organometal halide perovskite solar cells: degradation and stability. Energ Environ Sci, 2016, 9: 323–356
17 Alberti A, Deretzis I, Pellegrino G, *et al.* Similar structural dynamics for the degradation of $CH_3NH_3PbI_3$ in air and in vacuum. ChemPhysChem, 2015, 16: 3064–3071
18 Yantara N, Bhaumik S, Yan F, *et al.* Inorganic halide perovskites for efficient light-emitting diodes. J Phys Chem Lett, 2015, 6: 4360–4364
19 Kulbak M, Gupta S, Kedem N, *et al.* Cesium enhances long-term stability of lead bromide perovskite-based solar cells. J Phys Chem Lett, 2016, 7: 167–172
20 Kulbak M, Cahen D, Hodes G. How important is the organic part of lead halide perovskite photovoltaic cells? Efficient $CsPbBr_3$ Cells. J Phys Chem Lett, 2015, 6: 2452–2456
21 Stoumpos CC, Malliakas CD, Peters JA, *et al.* Crystal growth of the perovskite semiconductor $CsPbBr_3$: a new material for high-energy radiation detection. Cryst Growth Des, 2013, 13: 2722–2727
22 Eperon GE, Paternò GM, Sutton RJ, *et al.* Inorganic caesium lead iodide perovskite solar cells. J Mater Chem A, 2015, 3: 19688–19695
23 Choi H, Jeong J, Kim HB, *et al.* Cesium-doped methylammonium lead iodide perovskite light absorber for hybrid solar cells. Nano Energ, 2014, 7: 80–85
24 Xu J, Yin J, Xiao L, *et al.* Bromide regulated film formation of $CH_3NH_3PbI_3$ in low-pressure vapor-assisted deposition for efficient planar-heterojunction perovskite solar cells. Sol Energ Mater Sol Cells, 2016, 157: 1026–1037
25 Im JH, Luo J, Franckevičius M, *et al.* Nanowire perovskite solar cell. Nano Lett, 2015, 15: 2120–2126
26 Wong AB, Lai M, Eaton SW, *et al.* Growth and anion exchange conversion of $CH_3NH_3PbX_3$ nanorod arrays for light-emitting diodes. Nano Lett, 2015, 15: 5519–5524
27 Zhu H, Fu Y, Meng F, *et al.* Lead halide perovskite nanowire lasers with low lasing thresholds and high quality factors. Nat Mater, 2015, 14: 636–642
28 Horváth E, Spina M, Szekrényes Z, *et al.* Nanowires of methylammonium lead iodide ($CH_3NH_3PbI_3$) prepared by low temperature solution-mediated crystallization. Nano Lett, 2014, 14: 6761–6766
29 Liao JY, He JW, Xu H, *et al.* Effect of TiO_2 morphology on photovoltaic performance of dye-sensitized solar cells: nanoparticles, nanofibers, hierarchical spheres and ellipsoid spheres. J Mater Chem, 2012, 22: 7910–7918
30 Wu WQ, Huang F, Chen D, *et al.* Thin films of dendritic anatase titania nanowires enable effective hole-blocking and efficient light-harvesting for high-performance mesoscopic perovskite solar cells. Adv Funct Mater, 2015, 25: 3264–3272
31 Xu YF, Wu WQ, Rao HS, *et al.* CdS/CdSe co-sensitized TiO_2 nanowire-coated hollow spheres exceeding 6% photovoltaic performance. Nano Energ, 2015, 11: 621–630
32 Zhang D, Eaton SW, Yu Y, *et al.* Solution-phase synthesis of cesium lead halide perovskite nanowires. J Am Chem Soc, 2015, 137: 9230–9233
33 Bekenstein Y, Koscher BA, Eaton SW, *et al.* Highly luminescent colloidal nanoplates of perovskite cesium lead halide and their oriented assemblies. J Am Chem Soc, 2015, 137: 16008–16011
34 Protesescu L, Yakunin S, Bodnarchuk MI, *et al.* Nanocrystals of cesium lead halide perovskites ($CsPbX_3$, X = Cl, Br, and I): novel optoelectronic materials showing bright emission with wide color gamut. Nano Lett, 2015, 15: 3692–3696
35 Kim Y, Yassitepe E, Voznyy O, *et al.* Efficient luminescence from perovskite quantum dot solids. ACS Appl Mater Interfaces, 2015, 7: 25007–25013
36 Dastidar S, Egger DA, Tan LZ, *et al.* High chloride doping levels stabilize the perovskite phase of cesium lead iodide. Nano Lett, 2016, 16: 3563–3570
37 Hoffman JB, Schleper AL, Kamat PV. Transformation of sintered $CsPbBr_3$ nanocrystals to cubic $CsPbI_3$ and gradient $CsPbBr_xI_{3-x}$ through halide exchange. J Am Chem Soc, 2016, 138: 8603–8611
38 Wang F, Yu H, Xu H, *et al.* $HPbI_3$: a new precursor compound for highly efficient solution-processed perovskite solar cells. Adv Funct Mater, 2015, 25: 1120–1126
39 Liao JY, Lei BX, Kuang DB, *et al.* Tri-functional hierarchical TiO_2 spheres consisting of anatase nanorods and nanoparticles for high efficiency dye-sensitized solar cells. Energ Environ Sci, 2011, 4: 4079–4085
40 Pang S, Zhou Y, Wang Z, *et al.* Transformative evolution of organolead triiodide perovskite thin films from strong room-temperature solid–gas interaction between $HPbI_3$-CH_3NH_2 precursor pair. J Am Chem Soc, 2016, 138: 750–753
41 Eperon GE, Beck CE, Snaith HJ. Cation exchange for thin film lead iodide perovskite interconversion. Mater Horiz, 2016, 3: 63–71
42 Nedelcu G, Protesescu L, Yakunin S, *et al.* Fast anion-exchange in highly luminescent nanocrystals of cesium lead halide perovskites ($CsPbX_3$, X = Cl, Br, I). Nano Lett, 2015, 15: 5635–5640
43 Akkerman QA, D'Innocenzo V, Accornero S, *et al.* Tuning the optical properties of cesium lead halide perovskite nanocrystals by anion exchange reactions. J Am Chem Soc, 2015, 137: 10276–10281
44 Liao JF, Rao HS, Chen BX, *et al.* Dimension engineering on cesium lead iodide for efficient and stable perovskite solar cells. J Mater Chem A, 2017, 5: 2066–2072
45 Rao HS, Chen BX, Li WG, *et al.* Improving the extraction of photogenerated electrons with SnO_2 nanocolloids for efficient planar perovskite solar cells. Adv Funct Mater, 2015, 25: 7200–7207
46 Ye T, Fu W, Wu J, *et al.* Single-crystalline lead halide perovskite arrays for solar cells. J Mater Chem A, 2016, 4: 1214–1217

Acknowledgments This work was supported by the National Natural Science Foundation of China (91433109 and 51472274), Guangdong Province Universities and Colleges Pearl River Scholar Funded Scheme (2016), the Program of Guangzhou Science and Technology

(201504010031), the Fundamental Research Funds for the Central Universities, and the Natural Science Foundation of Guangdong Province (S2013030013474 and 2014A030313148).

Author contributions Kuang DB and Liao JF designed the experiments. Liao JF performed the material synthesis, measurements, data analysis and prepared the manuscript. Li WG, Rao HS, Chen BX, Wang XD and Chen HY provided helps in the characterizations and revision of the manuscript. All authors contributed to the general discussion.

Conflict of interest The authors declare that they have no conflict of interest.

Supplementary information Experimental details are available in the online version of the paper.

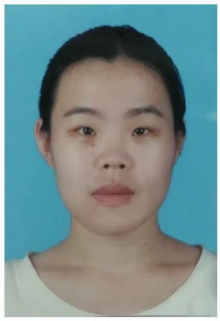

Jin-Feng Liao is a PhD student at the School of Chemistry of Sun Yat-sen University (SYSU). She received her Bachelor's degree from Sun Yat-sen Univerisity in 2015. Now her current research interest focuses on all inorganic perovskite and its application in perovskite solar cells.

Dai-Bin Kuang is a professor at the School of Chemistry of SYSU. Dr. Kuang received his PhD degree from SYSU in 2003. He worked at Max Planck Institute of Colloids and Interfaces (Germany) from 2003 to 2004 and then at Ecole Polytechnique Fédérale de Lausanne (Switzerland) from 2004 to 2008 as a postdoctoral researcher. His current research interest is in the field of new energy materials, focusing on functional nanostructured materials and their application in dye-sensitized/quantum dot-senstized solar cells, perovskite solar cells, photocatalysis and photoelechemical cells.

稳定的无机卤化铅铯纳米线钙钛矿电池

廖金凤, 李文广, 饶华商, 陈白雪, 王旭东, 陈洪燕, 匡代彬*

摘要 有机无机杂化钙钛矿因其优异的光电性能受到广泛关注, 但是其对湿度、热的不稳定性会限制钙钛矿电池的进一步发展. 本文通过简单的溶液浸泡法在导电基底上制备了尺寸为50–100 nm的全无机碘化铅铯纳米线, 并通过离子交换法将碘化铅铯置换成溴化铅铯纳米线. 文章通过X射线衍射谱、紫外可见吸收光谱、荧光发光光谱对I离子交换成Br离子过程进行了研究. 结果发现I-Br离子交换过程中伴随着晶体结构的变化, 起初的碘化铅铯为非钙钛矿结构, 离子交换后制备的溴化铅铯为钙钛矿结构. 本文将全无机卤化铅铯纳米线应用在钙钛矿电池器件中, 器件显示出优越的稳定性, 放置5500小时效率几乎未衰减.

Supplementary Information

Inorganic cesium lead halide $CsPbX_3$ nanowires for long-term stable solar cells

Jin-Feng Liao, Wen-Guang Li, Hua-Shang Rao, Bai-Xue Chen, Xu-Dong Wang, Hong-Yan Chen, Dai-Bin Kuang*

MOE Key Laboratory of Bioinorganic and Synthetic Chemistry, Lehn Institute of Functional Materials, School of Chemistry, Sun Yat-sen University, Guangzhou 510275, P. R. China.

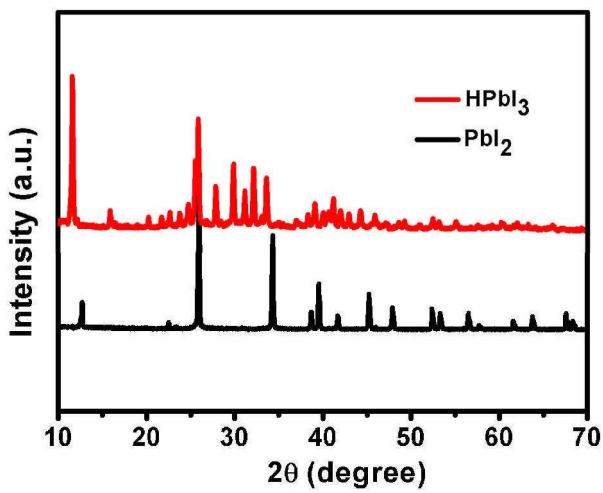

Figure S1 XRD patterns of $HPbI_3$ and PbI_2 powder.

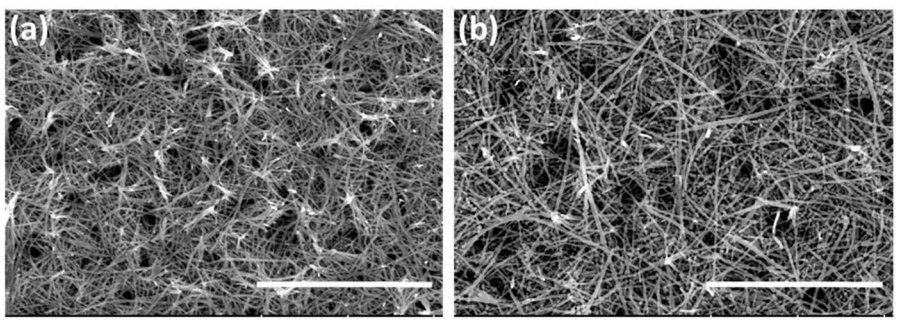

Figure S2 Plane-view SEM images of (a) $CsPbI_3$ nanowires film prepared by precursor $HPbI_3$ and (b) $CsPbBr_3$ nanowires film prepared by halide exchange of $CsPbI_3$ nanowires. Scale bars are 5 μm.

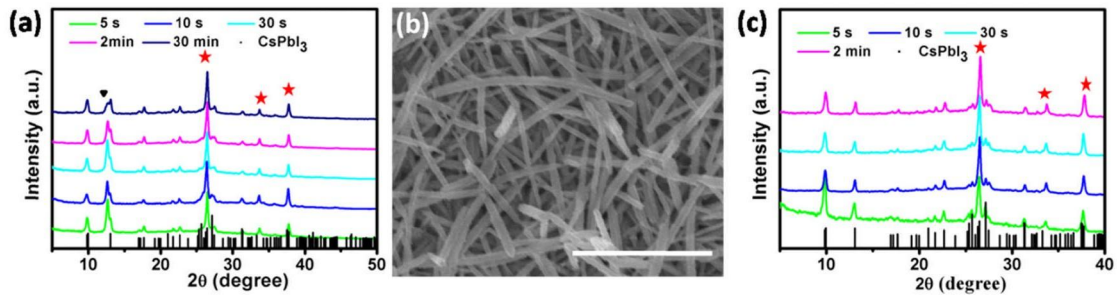

Figure S3 (a) XRD patterns of PbI_2 films and (c) $HPbI_3$ films dipped into CsI solution for varying time compared with the standard pattern of $CsPbI_3$. Peaks marked with an asterisk are XRD signals assigned to FTO substrate while marked with inverted triangle is XRD signal of PbI_2. (b) SEM image of PbI_2 film after dipped into CsI methanol solution. Scale bar is 1 μm.

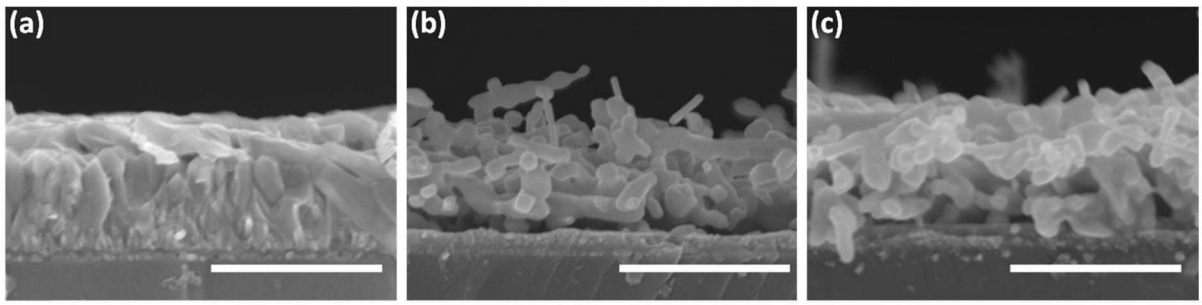

Figure S4 Cross-sectional SEM images of (a) $HPbI_3$ film, (b) $CsPbI_3$ nanowires film and (c) $CsPbBr_3$ nanowires film. Scale bars are 1 μm.

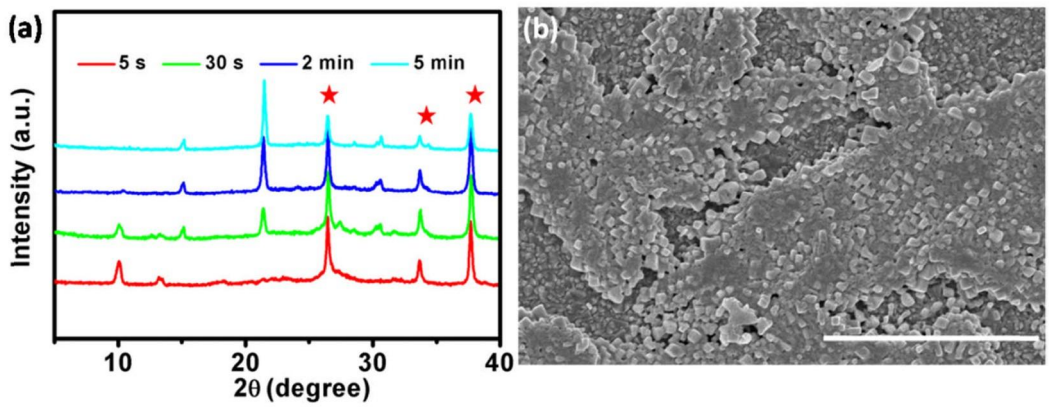

Figure S5 (a) XRD patterns of $HPbI_3$ films dipping into CsBr solution for varying time and (b) SEM image for the sample dipped for 2 min. Peaks marked with an asterisk are XRD signals assigned to FTO substrate. Scale bar is 5 μm.

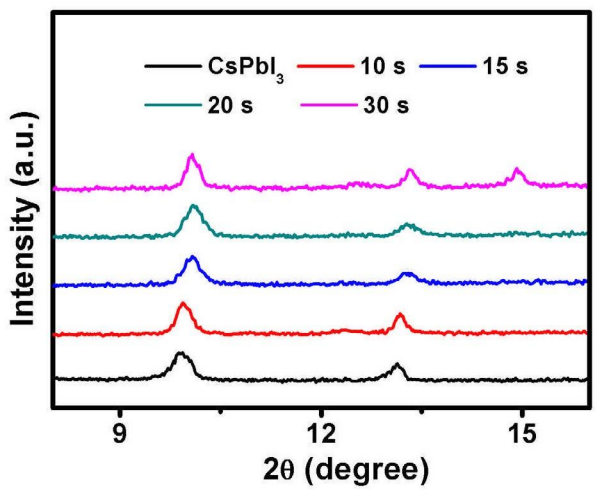

Figure S6 The magnification XRD patterns for $CsPbI_3$ nanowires film dipping time within 30 s.

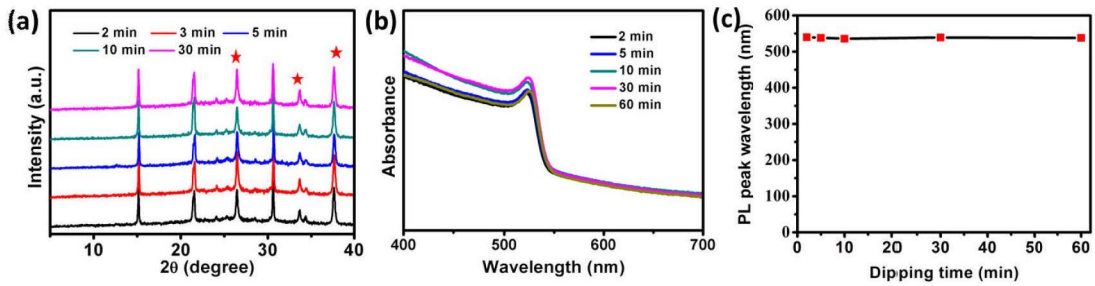

Figure S7 (a) XRD patterns, (b) UV-vis spectra and (c) PL speak wavelength of $CsPbI_3$ nanowires films dipped into CsBr methanol solution for a longer time (≥ 2 min) and annealed at 150 °C. Peaks marked with an asterisk are XRD signals assigned to FTO substrate.

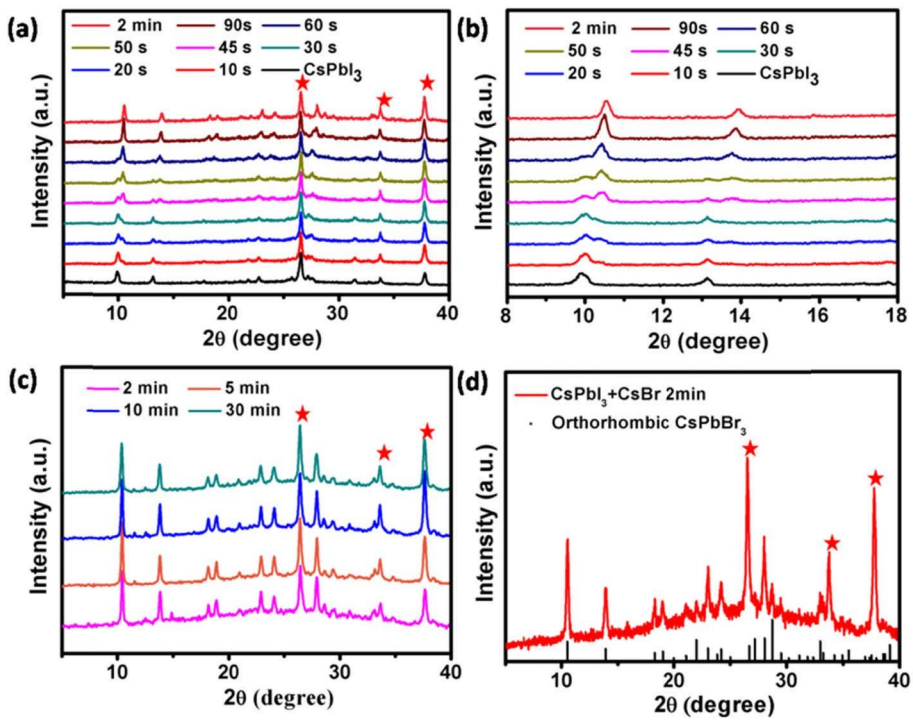

Figure S8 XRD patterns of (a) $CsPbI_3$ nanowires films dipped in CsBr solution for varying time without thermal treatment. (b) The magnification XRD patterns of a. (c) XRD patterns for $CsPbI_3$ nanowires films dipped into CsBr methanol solution for a longer time (≥ 2 min). (d) XRD pattern of $CsPbI_3$ nanowires film dipped in CsBr solution for 2 min compared with the standard XRD patterns of the nonperovskite $CsPbBr_3$. Peaks marked with an asterisk are XRD signals assigned to FTO substrate.

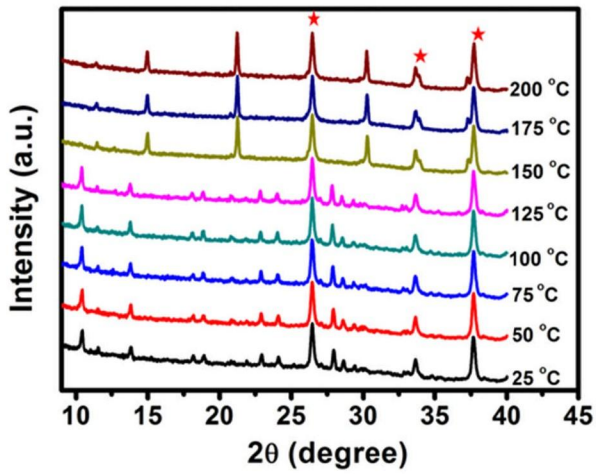

Figure S9 Temperature dependence XRD patterns of the as-formed nonperovskite $CsPbBr_3$. Peaks marked with an asterisk are XRD signals assigned to FTO substrate.

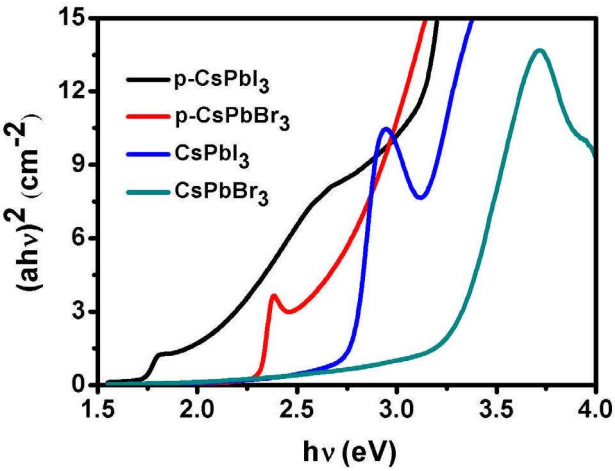

Figure S10 Tauc plots of $CsPbI_3$ and $CsPbBr_3$ with both non-perovskite and perovskite structure. (The prefix p presents a perovskite structure).

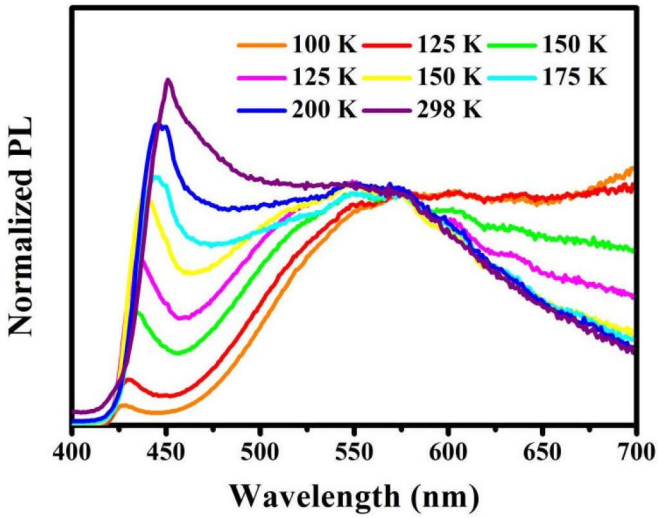

Figure S11 Temperature-dependent PL spectra of $CsPbI_3$ nanowires.

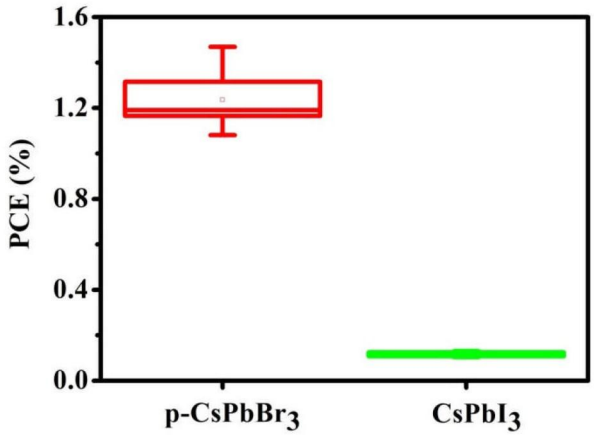

Figure S12 The box-chart image of power conversion efficiency for 10 devices based on p-$CsPbBr_3$ and $CsPbI_3$. (The prefix p presents a perovskite structure).

Table S1 Elemental analysis by energy dispersive X-ray spectra (EDX) for $HPbI_3$ powder

Element	Weight%	Atomic%
O K	5.20	12.73
I L	44.09	13.61
Pb M	25.16	4.76
Totals	100.00	

Table S2 Photovoltaic metrics of 8 devices based on cubed based $CsPbBr_3$ film

No.	V_{OC} (V)	J_{SC} (mA cm^{-2})	*FF*	PCE (%)
1	535	0.75	0.361	0.144
2	555	0.83	0.370	0.171
3	439	0.96	0.358	0.151
4	451	0.71	0.373	0.119
5	578	0.68	0.368	0.145
6	428	0.75	0.323	0.104
7	541	0.69	0.452	0.170
8	537	0.62	0.461	0.152
Average	508	0.75	0.383	0.145